*Geophysical Prospecting*, 1994, 42, 813–824

# Resistivity measurements on the sea bottom to map fracture zones in the bedrock underneath sediments[1]

O.B. Lile,[2] K.R. Backe,[2] H. Elvebakk[2] and J.E. Buan[3]

## Abstract

Refraction seismics with the shotpoints and the hydrophone cable on the sea-bottom, have become the standard geophysical method for investigating rock quality before constructing offshore tunnels in Norway. In connection with the construction of a sub-sea tunnel by the Norwegian Public Roads Administration, research work was carried out to compare two low-velocity zones, indicated by refraction seismics with other methods. A special resistivity cable for pole–dipole measurements on the sea-floor, with 10 m between the electrodes, was constructed. A 200 m long profile, crossing the two low-velocity zones, was measured with all combinations of electrode distances. The two zones were detected as low-resistivity zones. A special data processing technique to enhance the anomalies is described. Resistivity soundings in a seawater environment to detect fracture zones in the bedrock underneath the bottom sediments, are discussed. It is concluded that severely fractured zones, which may cause difficulties for the tunnel construction, can be detected both with sea-surface and sea-floor arrays using long electrode spacings.

## Introduction

In connection with the construction of sub-sea tunnels in Norway, refraction seismics have become the standard surveying method to map the rock quality along the tunnel trajectory. The hydrophone cable is deployed on the sea-bottom and the shots are fired close to the cable.

The Norwegian Public Roads Administration initiated some research in connection with the construction of the Maursund tunnel in northern Norway to compare the results from the refraction seismic survey with other methods of investigation. The Maursund Strait is situated between the island of Kågen and the Hamneidet

[1] Received December 1993, revision accepted June 1994.

[2] Department of Petroleum Engineering and Applied Geophysics, Norwegian Institute of Technology (NTH), University of Trondheim, N-7034 Trondheim, Norway.

[3] Norwegian Public Roads Administration, Oslo, Norway.

peninsula in Troms county. The strait is 1050 m wide and the water depth is approximately 35 m. The rock types are mica gneisses and quartzites with some amphibolites. The tunnel is 2095 m long.

## Previous surveys

Routine refraction seismics have previously been shot across the strait. Figure 1 shows an overview of the profiles with the seismic velocities in the upper part of the bedrock indicated along the profiles. Low-velocity sections are marked. Geological investigations in the area indicated that the strike directions of the major fracture zones were approximately east–west. It is fracture zones situated close to the shore that are particularly liable to create problems in the tunnel, since the

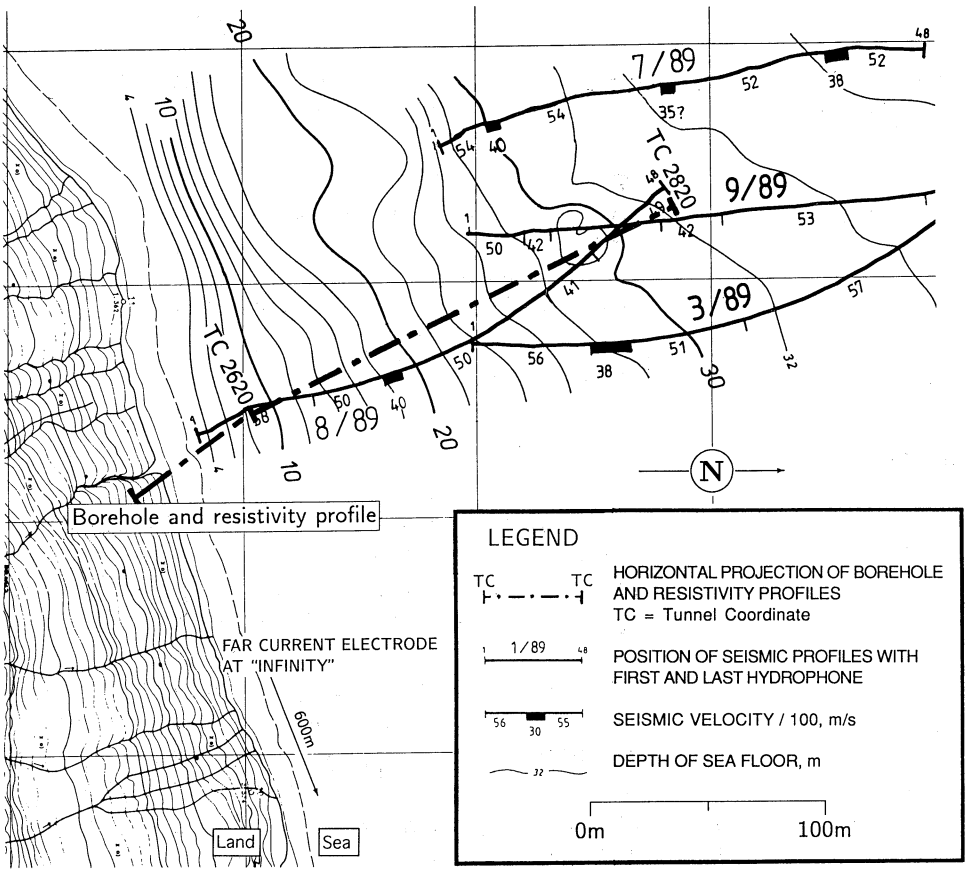


**Figure 1.** The southern shore of the Maursund Strait with the trace of the borehole and the resisitivity profile indicated. Seismic profiles with the seismic velocity in the upper part of the bedrock are marked.

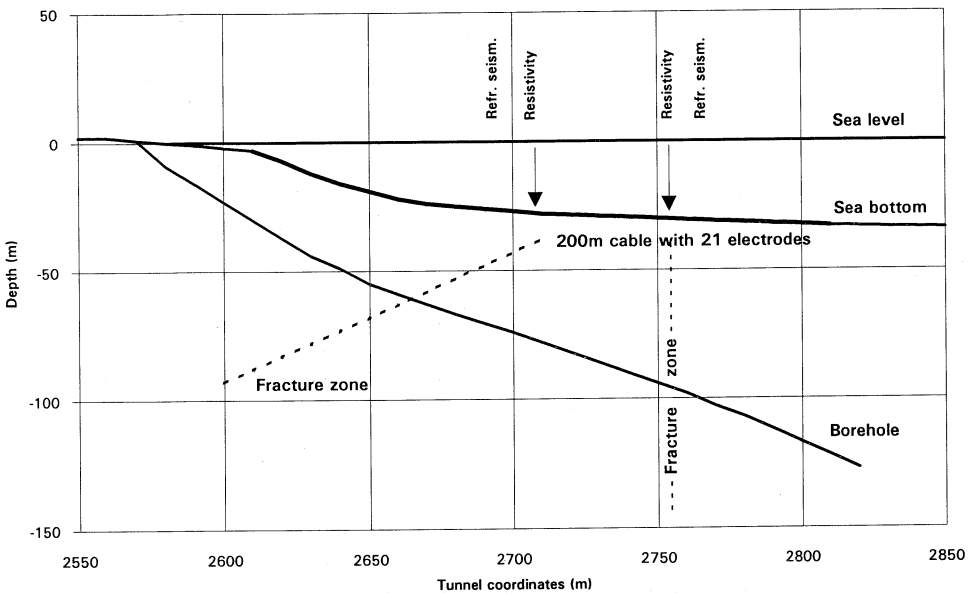


**Figure 2.** Cross-section through the resistivity profile and the borehole. The surface indications and the probable geometrical orientation of the two fracture zones are shown.

tunnel has not reached a sufficient depth to have a safe cover of rock between the sea-floor and the tunnel roof.

Two of the low-velocity zones, closest to the Hamneidet shore, are indicated on profile 8/89 as 40 (i.e. $V = 4000$ m/s) and 41 in Fig. 1. On profile 3/89, the outer fracture zone is marked 38. To investigate these two low-velocity zones, a deviated cored hole was drilled from the shore at Hamneidet to follow the tunnel trajectory through the low-velocity zones. The trace of the borehole is indicated in Fig. 1. The total length of the borehole was 292 m with an average dip of 27°. A cross-section through the hole is shown in Fig. 2. The core was logged and several fractured sections were mapped. However, because of the forced deviation of the borehole causing bending of the core barrel, much of the core was broken and clay had been washed away. It was therefore difficult to interpret which parts of the fractured core belonged to real fracture zones in the hole. Resistivity measurements in the 130 m open upper part of the hole helped to solve this problem.

## Resistivity measurements on the sea-bottom

Resistivity measurements in a seawater environment have been reported by Whiteley (1974), Lagabrielle and Teilhaud (1981), Lagabrielle (1983, 1984), Schrøder and Bidstrup (1987), Scott and Maxwell (1989), Lagabrielle and Chevalier (1991) and Schrøder (1992). All of these papers on underwater investigations were aimed

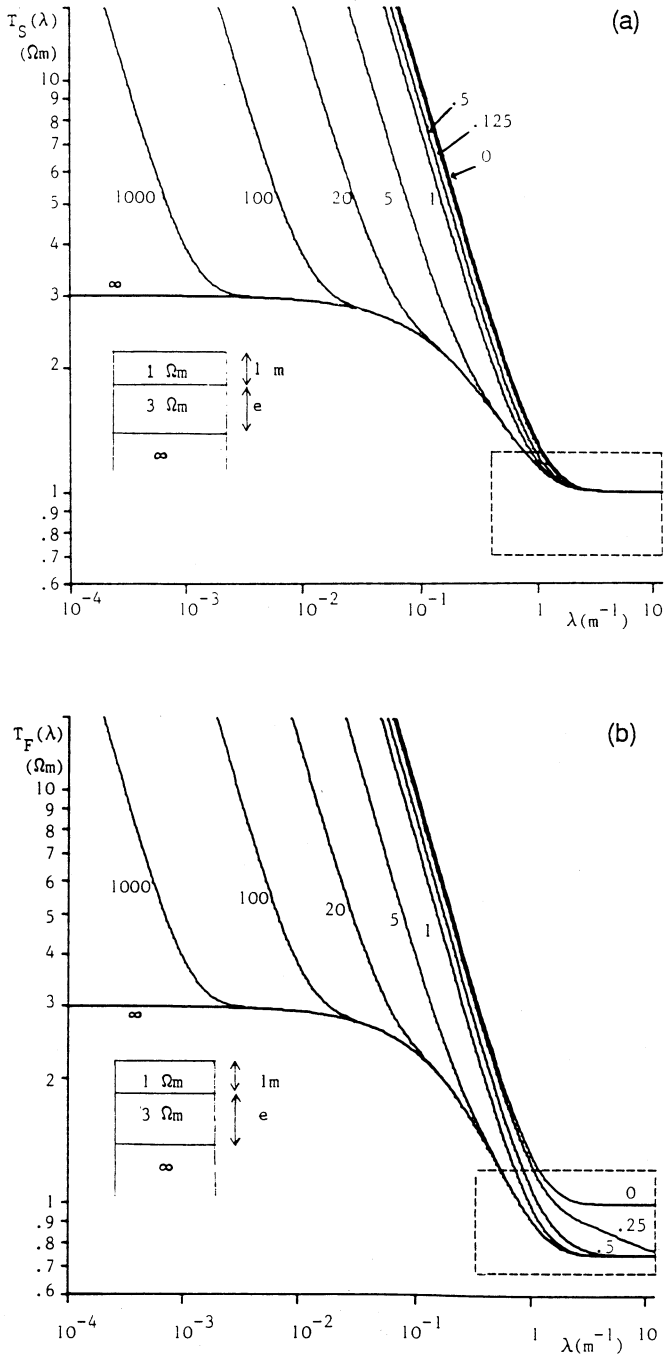


**Figure 3.** Resistivity transform of a three-layer model for electrode array on top of the first layer (a) and on top of the second layer (b). From Lagabrielle (1983).

at mapping sediment layers on the sea-bottom. Both Schrøder and Lagabrielle used a Wenner electrode configuration to obtain the highest possible potential differences, but only Lagabrielle used the electrode array on the sea-floor. Lagabrielle (1983) has written a good treatise on the theory of VES measurements on the sea-floor that can be utilized for any electrode configuration.

The most important result is the demonstration of the difference in apparent resistivity measured on the sea-surface and on the sea-floor. When the distance between the electrodes is very large compared to the sea depth, there is no difference in the measured resistivity between surface and bottom arrays. Short electrode distances, however, give a better resolution of shallow layers with a sea-floor array. Figure 3, showing the resistivity transform, is borrowed from Lagabrielle (1983) and illustrates this statement. The geological model represents the sea layer and one sediment layer on top of a resistive crystalline basement. Figure 3a represents measurements on the sea-surface and Fig. 3b represents sea-floor measurements. The different curves are for various thicknesses of the second layer of 3 Ωm, representing the bottom sediments. The parts of the curves within the box at large $\lambda$, represents the behaviour of the apparent resistivity curve for short spacings between the electrodes. Presented in this way, the behaviour of the apparent resistivity curve is not dependent on the electrode array type. The spreading of the curves in the sea-floor measurements illustrates the better resolution of the bottom layer. This is valid for short electrode spacings when the sediment thickness is smaller than the sea depth.

The aim of the resistivity measurements on the bottom of the Maursund Strait, was to find the low-velocity zones in the crystalline basement close to the southern shoreline and to investigate whether resistivity could classify the fracture zones with respect to possible problems in the tunnel construction. Combined resistivity profiling and vertical sounding was therefore performed along a profile on the sea-bottom, following the trace of the tunnel and the borehole trajectory. In order to obtain a good lateral resolution of resistivity, the pole–dipole configuration was chosen (Karous and Pernu 1985).

## Equipment, instruments and procedure

A special cable, 300 m long, was constructed for the measurements. One section of 200 m had 21 lead electrodes spaced at 10 m. Each of the electrodes was separately connected to a wire and a switch box via a 100 m long section of the cable. Weights of 0.5–1.0 kg were attached to the cable at each electrode to keep the cable on the sea-bottom in the strong tidal current that occurred in the strait. The switch box was placed on shore and the cable was deployed from a small boat. The far current electrode was situated in the sea, 20 m from the shore and 600 m to the east of the profile. The orientation of the profile was approximately N–S, at right angles to the shore-line. The profile is indicated in Fig. 1. A cross-section through the profile

and the borehole is shown in Fig. 2, illustrating the water depth and the position of the electrode section of the cable. The refraction seismics had indicated a sediment layer thickness of the order of 10 m.

The measurements were carried out using a frequency-domain McPhar IP/RP receiver and transmitter. The receiver has a frequency-locked amplifier and measures the voltage down to the microvolt range by a manually operated compensator. The transmitter current strength was approximately 1.5 A. The transmitter was not constructed for the low grounding resistance occurring in the sea. We therefore had to put a 150 Ω resistance in series. We used a frequency of 5 Hz for all the measurements. It would have been preferable to use a lower frequency, but because of the longer time involved taking the readings with the manually operated voltmeter at a lower frequency, the choice of 5 Hz was a compromise. All combinations of current poles and potential dipoles (10 m) were measured. The voltages that were measured ranged from 200 $\mu$V to 5 mV. Because of the low noise background, measurements in the microvolt range gave significant results.

## Data processing and interpretation

The results can be separated into two pseudosections, one with the current electrode to the north of the potential electrodes and one to the south. The apparent resistivities were calculated and plotted in the conventional manner, midway between and at a vertical coordinate equal to half the distance between the current electrode and the nearest potential electrode (Hallof 1967). Figures 4 and 5 show the two pseudosections.

It is well known that the conventional method of plotting the apparent resistivity values in a pseudosection distort the model picture. Using a dipole–dipole configuration, a vertical conductive plate in a homogeneous rock will image in a pseudosection as a dome-like structure. This is due to the electrode effect and can be seen in several publications of dipole–dipole pseudosections (e.g. Ward 1990). With a pole–dipole configuration, only half of the dome anomally will be visible. In Figs 4 and 5 the positions of the potential electrodes giving rise to the northern anomaly is indicated. The dipping of the anomaly is due to the plotting technique. By moving the current electrode towards the left in Fig. 4 the anomaly is indicated on the potential electrodes plot along the line dipping to the left. In Fig. 5 the plotting technique and moving the current electrode towards the right cause the anomaly dip to the right in the pseudosection. At short electrode spacings the anomaly is not clearly indicated. The shallowest indication of this zone is at coordinate 2755 m and at an approximate pesudodepth of 30 m. This coordinate of the shallowest indication is common for the two pole–dipole arrays. The positions of the current electrodes for the shallowest indication are also shown in Figs 4 and 5. At coordinate 2710 m and a pseudodepth of 30 m another low resistivity anomaly dipping at 45° in opposite directions is indicated in both Figs 4 and 5.

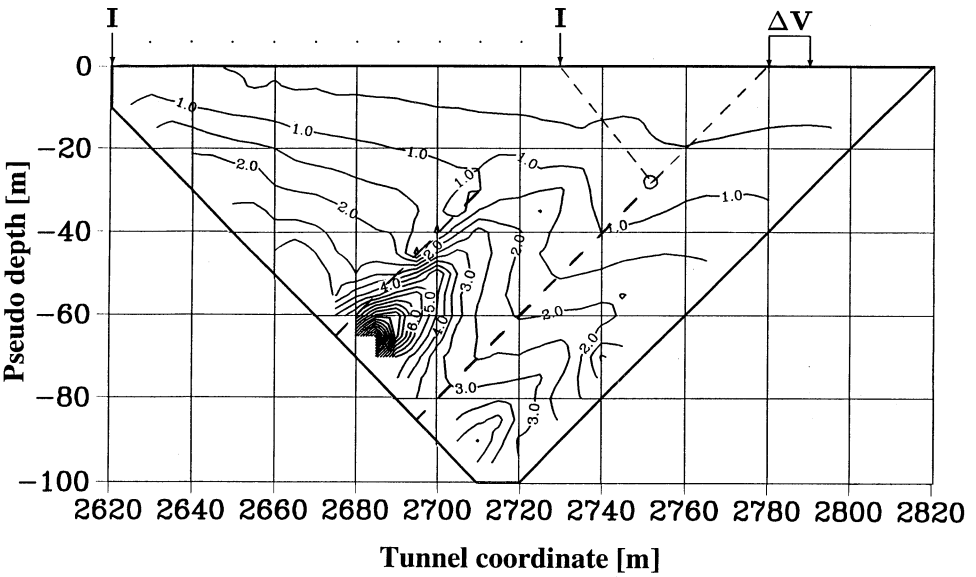


**Figure 4.** Pole–dipole resistivity pseudosection for measurements with the current electrode to the south of the potential electrodes.

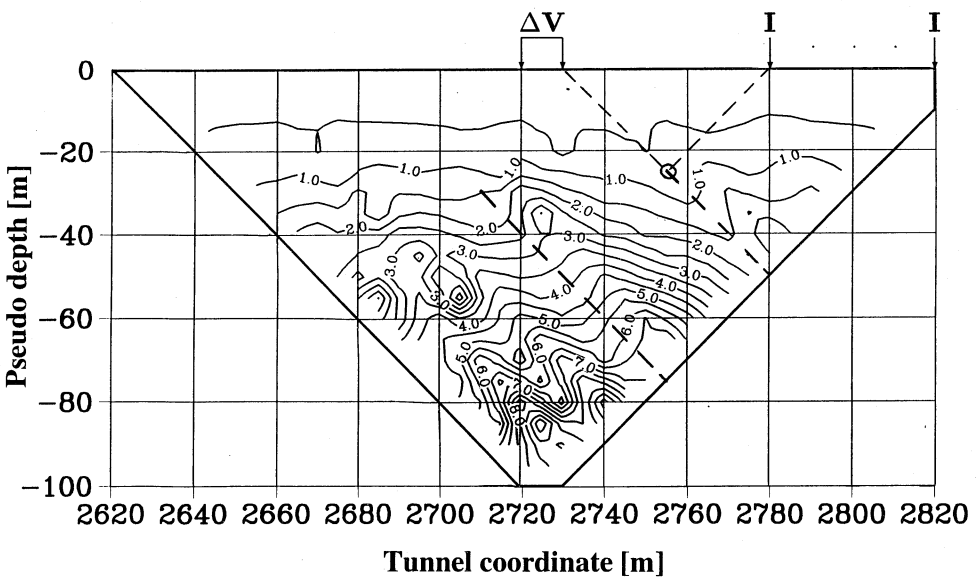


**Figure 5.** Pole–dipole resistivity pseudosection for measurements with the current electrode to the north of the potential electrodes.

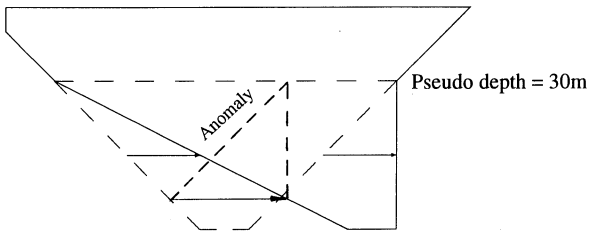


**Figure 6.** Outline of the data processing to correct for the electrode effect in the pseudosections.

We interpret the anomalies as low-resistivity zones in the bedrock that outcrop underneath the overburden. Due to the overburden thickness, the anomalies are not detected at the shortest electrode spacings. The pseudodepth to the top of the low-resistivity zone is 30 m but the real depth is about 10 m as we know from the refraction seismics. It is important to remember that the pseudodepth is only a plotting depth equal to half the distance between the current and the potential electrodes. This means that the low-resistivity structure in the bedrock (10 m deep) is not 'seen' by the pole–dipole configuration for electrode distances less than approximately 60 m.

In order to eliminate the electrode effect and make the pseudosection more comprehensible, each of the two standard pseudosections was processed separately. The processing consisted of moving the data points horizontally to correct for the dipping effect that the plotting technique created. Figure 6 illustrates the geometry

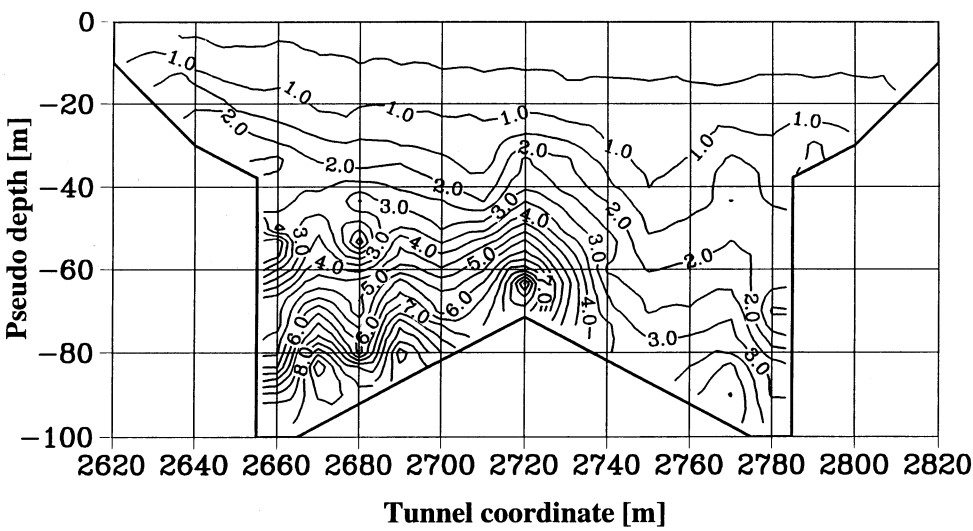


**Figure 7.** Resistivity pseudosection, stacked after correcting for electrode effects in Figs 4 and 5.

of the processing for the pseudosection in Fig. 4. Correspondingly, the data points in Fig. 5 were moved from right to left. Note that only the resistivity data obtained for electrode distances greater than 60 m, i.e. pseudo-depths greater than 30 m, were moved. In this way the anomalies in the two pseudosections were transformed into vertical anomalies situated at the same coordinates. Finally, the data points in the two pseudosections were stacked to enhance the anomalies. The result is shown in Fig. 7. The northern zone, indicated at the coordinate 2750 m, now appears as a vertical low-resistivity zone and can be seen for electrode distances up to 180 m, i.e. at a plotting depth or pseudo-depth of 90 m. The anomaly at the coordinate 2710 m shows a tendency to dip towards the south. This is in accordance with the measurements in the borehole where a low-resistivity zone was found at approximately 2670 m (Fig. 2). This was also the only resistivity anomaly that could be correlated with the southern anomaly at 2710 m, interpreted as a low-resistivity zone dipping approximately 40° to the south. In Fig. 7, low-resistivity indications can also be observed at the coordinates 2680 m and 2655 m in the deeper part of the pseudosection. Later mapping in the tunnel also found these indications significant for water leakages and the precautions that had to be taken (Hagelia 1994).

## Discussion

The refraction seismic measurements on the sea-bottom indicated low-velocity zones at tunnel coordinates 2690 m and 2770 m. As can be seen in Fig. 1, the refraction seismic profile was not located exactly above the tunnel and the borehole trajectory. Therefore, a certain degree of inaccuracy in the coordinate determination must be accepted. The difference in position of 15–20 m between the seismic and the resistivity zones, may be due to the deployment of the resistivity cable on the sea-bottom. The current in the strait made it difficult to position the cable precisely and the actual position was not measured after deployment. In spite of this inaccuracy, the difference is not very large from a practical point of view.

As mentioned above, the applied frequency for the resistivity measurements was 5 Hz. This might give problems regarding depth of penetration in the highly conducting environment. However, the combined pole–dipole resistivity profiling and depth sounding appeared to be able to map lateral resistivity variations through the 10–15 m overburden.

The maximum depth of penetration or skin depth $d$ is by definition the depth at which the amplitude of a plane wave is attenuated to approximately 37% (1/e) of the amplitude at the surface, and is given by

$$d = (\rho_s/\pi\mu f)^{1/2},$$

where $\rho_s$ is the resistivity of the sediments, $\mu$ is the magnetic permeability of the sediments, usually equal to $\mu_0 = 4\pi \times 10^{-7}$ $\mathrm{Hm}^{-1}$, and $f$ is the frequency.

The resistivity of seawater at a temperature of 5°C, is 0.30 Ωm. Assuming a porosity of 40% in the unconsolidated sediments and applying Archies law (Archie

1942), we get:

$$\rho_s = \rho_w/\phi^2 \cong 2\ \Omega\text{m},$$

where $\rho_s$ is the resistivity of the water-saturated porous sediment layer, $\rho_w$ is the resistivity of the pore water, and $\phi$ is the porosity of the sediment.

Using a frequency of 5 Hz, the skin depth $d$ is then approximately 320 m.

This shows that the limiting factor for the depth of investigation in the Maursund Strait was the distance between the electrodes in the array. The maximum distance we could use was limited by the length of the cable, 200 m, giving a maximum depth of investigation on the order of 30 m.

Electromagnetic (EM) induction may be a problem under these conductive conditions. When using long arrays with a high frequency, part of the resistivity reading is due to EM induction when the environment has low resistivity. In this case the EM induction appeared to be fairly constant along the profile. One may, however, suspect that some high apparent resistivity points in the pseudosection are caused by high local EM induction. Examples of this may be seen in the deeper parts of Figs 4 and 5.

The general increase of apparent resistivity versus depth is due to the resistive bedrock. Figure 8 shows the calculated resistivity transform for the situation in the Maursund Strait. The model is as follows:
Seawater layer: $t = 30$ m, $\rho = 0.3\ \Omega$m, bottom sediment layer: $t = 0$, 10, 30, 150 and 600 m, $\rho = 2\ \Omega$m, bedrock half-space: $\rho = 1000\ \Omega$m.

As can be seen from Fig. 3b, valid for an electrode array on the sea-bottom, the apparent resistivity $\rho_a$ for small electrode spacings (large $\lambda$) is the result of two parallel resistivities (Lagabrielle 1983), i.e.

$$\rho_a = (\rho_w \rho_s)/(\rho_w + \rho_s)$$

or

$$\sigma_a = (\sigma_w + \sigma_s),$$

where the apparent conductivity $\sigma_a = 1/\rho_a$, the water conductivity $\sigma_w = 1/\rho_w$, and the sediment conductivity $\sigma_s = 1/\rho_s$.

Using the actual resistivity for seawater and the assumed resistivity for the bottom sediments, we get the asymptotic value of measured resistivity at small electrode distances, i.e. $\rho_a = 0.26\ \Omega$m.

When the sediment thickness is zero, the low conductivity of the bedrock will not contribute and the electrode array on the sea-floor will measure the resistivity of seawater, i.e.

$$\rho_a = 0.3\ \Omega\text{m}.$$

When the depth of the sea is greater than the thickness of the bottom sediments, the seawater conductivity is so dominant for small electrode distances (large $\lambda$) that

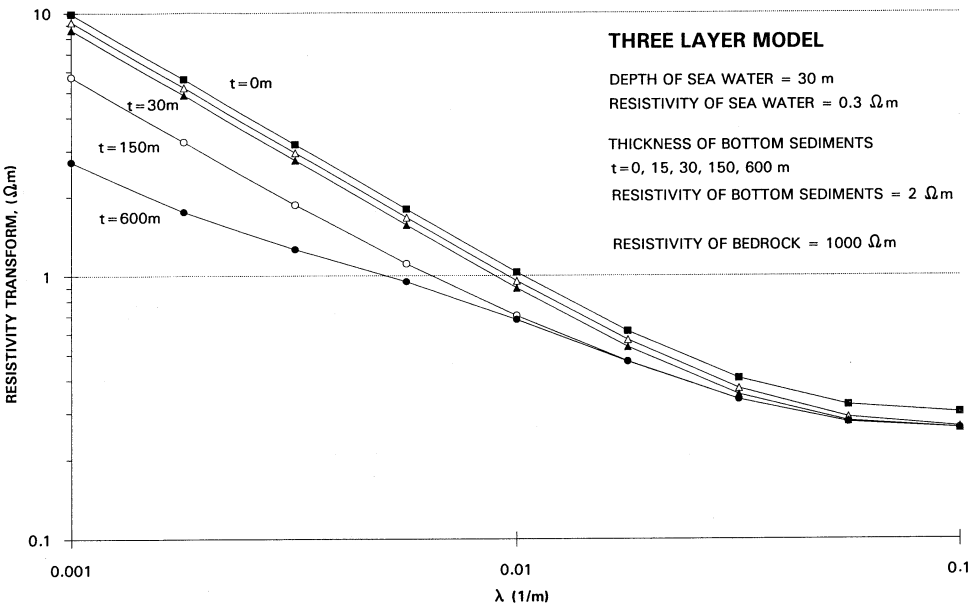


**Figure 8.** Resistivity transform curves calculated for the sea-floor measurements in the Maursund Strait.

the thickness of the bottom sediments does not have any significant influence on the apparent resistivity.

At the other end of the $\lambda$ axis, i.e. for large electrode spacings, a spreading of the resistivity transform curves can be observed for sediment thicknesses larger than the sea depth.

The lower apparent resistivities which have been observed over fracture zones in the Maursund Strait for large electrode spacings, may thus be explained by an apparent increase of the bottom sediment thickness. The low-resistivity fracture zones in the bedrock appear as an increase of the sediment thickness. Referring to Fig. 3, it can be concluded that the detection of the fracture zones in the Maursund Strait using large electrode spacings, could as well have been obtained with the electrode array on the sea-surface. For operational reasons, however, measurements with a surface array in this case would have been very difficult.

## Conclusion

Resistivity measurements, with the electrode array situated on the sea-floor, have detected low-resistivity fracture zones in a high-resistivity basement underneath 10 m of sediment cover. The high conductivity of sea-water dominates the measured resistivities at small electrode spacings. Therefore, the resolution of the sediment thickness is poor. For large electrode spacings the apparent resistivities measured with arrays on the sea-surface and on the sea-floor are equal. The detection of

fracture zones underneath bottom sediments may be explained by an apparent increase of the sediment thickness. Severely fractured and broad zones that may cause difficulties for tunnel construction, are therefore likely to be indicated by electrical resistivity measurements. Resistivity anomalies may thus be used for classification of fracture zones in the same way as seismic velocities are used today.

## Acknowledgements

We thank the Norwegian Public Roads Administration for financing these investigations. Thanks are also due to I. Reiertsen for valuable help during the field work.

## References

Archie G.E. 1942. The electrical resistivity log as an aid in determining some reservoir characteristics. *Transactions of the AIME* **146**, 54–62.

Hagelia P. 1994. Detection of leakage sensitive joint systems using resistivity measurements in connection with sub-sea tunnels. In: Proceedings of the 3rd symposium on strait crossings (ed. J Krokeborg), Ålesund, Norway, pp. 371–378.

Hallof P.G. The use of induced polarization measurements to locate massive sulphide mineralization in environments in which EM methods fail. In: *Mining and Groundwater Geophysics/1967* Economic Geology Report no. 26. Geological Survey of Canada, (ed. L.W. Morley), pp. 302–309.

Karous M. and Pernu T.K. 1985. Combined sounding-profiling resistivity measurements with three-electrode arrays. *Geophysical Prospecting* **33**, 447–459.

Lagabrielle R. 1983. The effect of water on direct current resistivity measurement from the sea, lake or river floor. *Geoexploration* **21**, 165–170.

Lagabrielle R. 1984. La prospection électrique par courant continu en mer. *Bull. Liaison Labo. P. et Ch.* **132**, 6/8, 5–11.

Lagabrielle R. and Chevalier M. 1991. Prospection électrique par courant continu en site aquatique. *Bull. Liaison Labo. P. et Ch.* **171**, 57–62.

Lagabrielle R. and Teilhaud's. 1981. Prospection de gisements alluvionnaires en site aquatique par profils continue de résistivité au fond de léau. *Bull. Liaison Labo. P. et Ch.* **114**, 17–24.

Schrøder N. 1992. Resistivity at Sea. In: *Handbook of Geophysical Exploration at Sea*, 2nd edn, (ed. R.A. Geyer), pp. 323–335. CRC Press.

Schrøder N. and Bidstrup T. 1987. Resistivity at sea: inversion and interpretation of measurements. 57th SEG meeting, New Orleans, Expanded Abstracts, 94–95.

Scott W.J. and Maxwell F.F. 1989. Marine resistivity survey for granular materials. *Beaufort Sea. Canadian Journal of Exploration Geophysicists* **25**, 104–114.

Ward S.H. 1990. Resistivity and induced polarization methods. In: *Geotechnical and Environmental Geophysics. Volume I: Review and Tutorial* (ed. S.H. Ward). Investigations in Geophysics 5. Society of Exploration Geophysicists, 147–189.

Whiteley R.J. 1974. Design and preliminary testing of a continuous offshore resistivity method. *Bulletin of the Australian Society of Geophsicists* **5**, 9–14.